SIAM J. APPLIED DYNAMICAL SYSTEMS
Vol. 11, No. 4, pp. 1402–1424

On 3-Parameter Families of Piecewise Smooth Vector Fields in the Plane*

Claudio A. Buzzi†, Tiago de Carvalho‡, and Marco A. Teixeira§

Abstract. This paper is concerned with the local bifurcation analysis around typical singularities of piecewise smooth planar dynamical systems. Three-parameter families of a class of nonsmooth vector fields are studied, and the bifurcation diagrams are exhibited. Our main results describe a particular unfolding of the so-called *fold-cusp* singularity by means of the variation of 3 parameters.

Key words. nonsmooth vector field, bifurcation, canard cycle, limit cycle, pseudoequilibrium

AMS subject classifications. 34A36, 37G10, 37G05

DOI. 10.1137/100817309

1. Introduction.

Nonsmooth dynamical systems (NSDSs, for short) have become certainly one of the common frontiers between mathematics and physics or engineering. Problems involving impact or friction are piecewise-smooth, as are many control systems with thresholds. Many authors have contributed to the study of Filippov systems (see, for instance, [7] and [10] about details of these multivalued vector fields). One of the starting points for a systematic approach to the geometric and qualitative analysis of NSDSs is [12], on smooth systems in 2-dimensional manifolds with boundary. The generic singularities that appear in NSDSs, to the best of our knowledge, were first studied in [13]. Bifurcations and related problems, possibly involving sliding regions, were studied in papers like [6, 8, 1, 2]. The classification of codimension-1 local and some global bifurcations for planar systems was given in [11]. In [9] (respectively, [5]) planar codimension-2 singularities (respectively, 3-parameter families) were discussed, and it was shown how to construct the homeomorphisms which lead to topological equivalences between two NSDSs when the discontinuity set is a planar smooth curve. See [14] or [3] (and references therein) for a survey on NSDSs.

The specific topic addressed in this paper is the qualitative analysis of *fold-cusp singularities* of NSDSs, where a fold and a cusp coincide. Moreover, the bifurcation diagrams of particular unfoldings are exhibited. Our main concern is to analyze how the bifurcation whose configuration is shown in Figure 4 falls within the bifurcation diagram of a fold-cusp singularity. This is not an easy task, since it was necessary to add into the unfolding of the singularity a C^1-bump function. Moreover, the application of this tool through a C^r-bump function, with $r > 1$, did not work. This fact escaped our initial intuition. In fact, some obstructions in the

*Received by the editors December 7, 2010; accepted for publication (in revised form) by H. Kokubu July 24, 2012; published electronically October 18, 2012. The first and the third authors are partially supported by FAPESP-BRAZIL grant 2007/06896-5.

http://www.siam.org/journals/siads/11-4/81730.html

†IBILCE-UNESP, CEP 15054-000, S. J. Rio Preto, São Paulo, Brazil (buzzi@ibilce.unesp.br).

‡FC-UNESP, CEP 17033-360, Bauru, São Paulo, Brazil (tcarvalho@fc.unesp.br). This author was partially supported by FAPESP-BRAZIL grants 2007/08707-5, 2010/18190-2, and 2012/00481-6.

§IMECC-UNICAMP, CEP 13081-970, Campinas, São Paulo, Brazil (teixeira@ime.unicamp.br).

Figure 1. *Fold-cusp singularities: An invisible one on the left, and a visible one on the right.*

completeness of the bifurcation diagram occur when C^2 perturbations of the original system are considered instead of C^1 perturbations. Thus the unfolding considered is very special and does not fit within the usual sense of generic dynamical systems theory.

We consider a codimension-1 manifold Σ of $\mathbb{R}^2$ given by $\Sigma = f^{-1}(0)$, where $f : V \to \mathbb{R}$ is a smooth function having $0 \in \mathbb{R}$ as a regular value (i.e., $\nabla f(p) \neq 0$ for any $p \in f^{-1}(0)$), and V is an arbitrarily small neighborhood of $0 \in \mathbb{R}^2$. We call Σ the *switching manifold*, that is, the separating boundary of the regions $\Sigma^+ = \{q \in V | f(q) \geq 0\}$ and $\Sigma^- = \{q \in V | f(q) \leq 0\}$. In this paper we assume that Σ is represented, locally around the origin of $\mathbb{R}^2$, by the function $f(x, y) = y$.

We denote by $Z = (X, Y)$ the vector field

$$Z(x,y) = \begin{cases} X(x,y) & \text{for } (x,y) \in \Sigma^+, \\ Y(x,y) & \text{for } (x,y) \in \Sigma^-, \end{cases} \tag{1.1}$$

where $X = (f_1, g_1)$, $Y = (f_2, g_2)$ are smooth vector fields defined in V. The trajectories of Z are solutions of $\dot{q} = Z(q)$ in the sense of Filippov; i.e., we will accept it to be multivalued at points of Σ. The basic results of differential equations, in this context, were stated by Filippov in [7].

1.1. Setting the problem.

In short, our goal is to study the local dynamics of some class of systems $Z = (X, Y)$ at $0 \in \mathbb{R}^2$. Points where the vector field X (respectively, Y) has a quadratic (respectively, cubic) tangency to Σ are called Σ-*fold points* (respectively, Σ-*cusp points*). A Σ-fold point is *visible* (respectively, *invisible*) if the trajectory that touches Σ is visible (respectively, invisible) (for a precise definition see section 2).

Following Theorem 2 of [15], we can conclude that any $X \in \Sigma^+$ presenting a Σ-fold point is C^0-orbitally equivalent (according to Definition 2.2) to the normal form $X_0(x, y) = (\rho_1, \rho_2 x)$ with $\rho_1 = \pm 1$ and $\rho_2 = \pm 1$.

Following [12], we can derive that any $Y \in \Sigma^-$ presenting a Σ-cusp point is C^0-orbitally equivalent (according to Definition 2.2) to the normal form $Y_0(x, y) = (\rho_3, \rho_4 x^2)$ with $\rho_3 = \pm 1$ and $\rho_4 = \pm 1$.

In this paper we consider the *fold-cusp singularity*; i.e., 0 is a Σ-fold point of X and a Σ-cusp point of Y (see Figure 1).

We start with the normal form of an invisible (respectively, visible) fold-cusp singularity given by

$$W = \begin{cases} X = \begin{pmatrix} 1 \\ \upsilon x \end{pmatrix} & \text{if } y \geq 0, \\ Y = \begin{pmatrix} \upsilon \\ -x^2 \end{pmatrix} & \text{if } y \leq 0, \end{cases}$$

where $\upsilon = -1$ (respectively, $\upsilon = 1$).

In [9] the analysis of the bifurcation diagram of the 2-parameter family

$$W_{\mu,\epsilon} = \begin{cases} \overline{X_\mu} = \begin{pmatrix} 1 \\ -x+\mu \end{pmatrix} & \text{if } y \geq 0, \\ \overline{Y_\epsilon} = \begin{pmatrix} -1 \\ -x^2+\epsilon \end{pmatrix} & \text{if } y \leq 0 \end{cases}$$

of NSDSs presenting an invisible fold-cusp singularity is performed. A challenging problem is to extend the analysis of [9] in answering the following question: Can we find families of NSDSs presenting fold-cusp singularities whose dynamics is richer than the family exhibited in [9]? Can we observe a configuration like that in Figure 2?

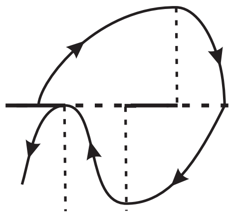

Figure 2. *Configuration nearby $Z_{0,0,0}$ not observed in* [9].

In order to detect a larger range of topological behaviors near an invisible fold-cusp singularity we have to refine the analysis done in [9]. This refinement can be obtained by adding a bump function to the expression of the NSDS.

Specifically, we distinguish the following cases (see Figure 1):

• Unfolding of an invisible fold-cusp singularity:

$$Z_{\lambda,\beta,\mu} = \begin{cases} X_\lambda = \begin{pmatrix} 1 \\ -x+\lambda \end{pmatrix} & \text{if } y \geq 0, \\ Y_{\beta,\mu} = \begin{pmatrix} -1 \\ -x^2+\beta-\frac{\partial B}{\partial x}(x,\beta,\mu)) \end{pmatrix} & \text{if } y \leq 0, \end{cases} \tag{1.2}$$

where $(\lambda, \beta, \mu) \in (-\lambda_0, \lambda_0) \times (-\beta_0, \beta_0) \times (-\mu_0, \mu_0)$, with $\lambda_0 > 0$, $\beta_0 > 0$, and $\mu_0 > 0$ sufficiently small, and B is a *bump function* such that $B(x, \beta, \mu) = 0$ if $\beta \leq 0$ and

$$B(x,\beta,\mu) = \begin{cases} 0 & \text{if } x < -\sqrt{\beta} \text{ or } x > 4\sqrt{\beta}, \\ B_1(x,\beta) + f(\beta,\mu) & \text{if } -\sqrt{\beta} \leq x \leq \sqrt{\beta}, \\ B_2(x,\beta) + f(\beta,\mu) & \text{if } \sqrt{\beta} < x \leq 4\sqrt{\beta} \end{cases} \tag{1.3}$$

if $\beta > 0$, where

$$B_1(x,\beta) = \frac{-3}{128\beta}\begin{pmatrix} (x+\sqrt{\beta})^3(x^2(208+3\beta)- \\ 4x\sqrt{\beta}(176+15\beta)+\beta(688+93\beta)) \end{pmatrix},$$
$$B_2(x,\beta) = \frac{-1}{48\beta}\begin{pmatrix} (x-4\sqrt{\beta})^3((x^2+\beta)(-16+9\beta)- \\ 2x\sqrt{\beta}(16+15\beta)) \end{pmatrix},$$

and

$$f(\beta,\mu) = \frac{\mu}{48}\begin{pmatrix} -8\beta(128+3\beta)\mu\sqrt{\beta}(256+63\beta)\mu-(-64+45\beta)\mu^2- \\ \beta^{-1/2}(80+3\beta)\mu^3+\beta^{-1}(-16+9\beta)\mu^4) \end{pmatrix}.$$

Now we list two important features of the bump function B that appears in (1.2).

1. It has exactly one point of local minimum in the interval $(-\sqrt{\beta}, 4\sqrt{\beta})$. This point is located at $x_0 = \sqrt{\beta}$. As a consequence, $Y_{\beta,\mu}$ has just one invisible Σ-fold point when $\beta > 0$.
2. $F(3\sqrt{\beta}+\mu) = 0$ (see Figure 3). By means of this last property the orbit-arc of $Y_{\beta,\mu}$ that has a quadratic contact with Σ at $q_0 = (-\sqrt{\beta}, 0)$ turns to collide with Σ at the point $q_1 = (3\sqrt{\beta}+\mu, 0)$. So, the first coordinate of q_1 is bigger (respectively, smaller) than $3\sqrt{\beta}$ as μ is bigger (respectively, smaller) than 0.

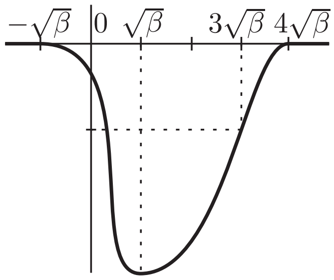

Figure 3. *Graph of B.*

Observe that $Y_{\beta,0}$ is not the same as $\overline{Y_\varepsilon}$ for $\varepsilon = \beta$.

It is worth saying that in this paper the bifurcation diagram of (1.2) is such that, under the conditions $\beta = \mu^2$ and $\mu \leq 0$, the diagram obtained coincides with the diagram presented in [9].

We mention an interesting phenomenon illustrated in Figure 4 that occurs in (1.2) when $\beta > 0$. We note, simultaneously, a two-fold singularity and a loop passing through the visible Σ-fold point of Y.

• Unfolding of a visible fold-cusp singularity:

$$Z_{\lambda,\beta} = \begin{cases} X_\lambda = \begin{pmatrix} 1 \\ x-\lambda \end{pmatrix} & \text{if } y \geq 0, \\ Y_\beta = \begin{pmatrix} 1 \\ -x^2+\beta \end{pmatrix} & \text{if } y \leq 0, \end{cases} \tag{1.4}$$

where $(\lambda,\beta) \in (-\lambda_0,\lambda_0)\times(-\beta_0,\beta_0)$, with $\lambda_0 > 0$ and $\beta_0 > 0$ sufficiently small.

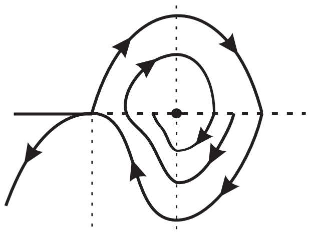

Figure 4. *The local and the global bifurcations observed in* (1.2) *when* $\beta > 0$, $\lambda = \sqrt{\beta}$, *and* $\mu = 0$.

Remark 1.1. *Note that in* (1.2) *and* (1.4) *the perturbations considered depend only on the variable* x. *The local geometry of an NSDS presenting a cusp-fold singularity becomes rather different if perturbations involving the variables* x *and* y *are admitted. Moreover, another important restriction on the perturbation considered here is that the second component of* Y_ϵ *is constrained to have only one maximum and one minimum. In general the second component of the perturbed system could have several minima and maxima since it is* C^1 *but not* C^2 *small. In addition, in the* C^2 *topology, it happens that* $Y_{\beta,\mu} \to Y_{\beta,0}$ *as* $\mu \to 0$, *but it is not the case that* $Y_{\beta,0} \to Y_{0,0}$ *as* $\beta \to 0$.

1.2. Statement of the main results. Theorems 1, 2, and 3 pave the way for the proof of Theorem A. Theorem B is self-contained.

Theorem 1. *If* $\mu = 0$ *in* (1.2), *then its bifurcation diagram in the* (λ, β)*-plane contains essentially* 17 *distinct phase portraits (see Figure* 23*).*

It is easy to see that in a neighborhood of $Z_{\lambda,\beta,0}$ in (1.2), there exist cases not covered by Theorem 1. Because of this, the next two theorems are necessary.

Theorem 2. *There exists* $\mu_0 > 0$ *such that if* $0 < \mu < \mu_0$ *in* (1.2), *then its bifurcation diagram in the* (λ, β)*-plane contains essentially* 19 *distinct phase portraits (see Figure* 25*).*

Theorem 3. *There exists* $\mu_0 > 0$ *such that if* $-\mu_0 < \mu < 0$ *in* (1.2), *then its bifurcation diagram in the* (λ, β)*-plane contains essentially* 19 *distinct phase portraits (see Figure* 25*).*

Finally, we are in position to state the main results of the paper.

Theorem A. *The bifurcation diagram of* (1.2) *exhibits* 55 *distinct cases representing* 23 *distinct phase portraits (see Figure* 27*).*

Theorem B. *The bifurcation diagram of* (1.4) *exhibits* 11 *distinct phase portraits (see Figure* 33*).*

The paper is organized as follows. In section 2 we present some basic elements of the theory of NSDSs. In sections 3, 4, and 5 we pave the way for the proofs of the main results of the paper (Theorems A and B). Section 6 is devoted to proving Theorem A and exhibiting the bifurcation diagram of (1.2). In section 7, the proof of Theorem B and the bifurcation diagram of (1.4) are presented, and in section 8 some concluding remarks are discussed. In our paper we basically follow the terminology and the approach of [11] or [9], and no sophisticated tools are needed.

2. Preliminaries.

Designate by χ the space of C^1-vector fields on $V \subset \mathbb{R}^2$ endowed with the C^1-topology. Call $\Omega = \chi \times \chi$ the set of all $Z = (X, Y)$ as defined in section 1. We endow Ω with the product topology.

Definition 2.1. *A k-*parameter family *of elements in Ω is a C^0-mapping*

$$\begin{array}{llll} \zeta : & S^k & \longrightarrow & \Omega, \\ & \varrho = (\varrho_1, \varrho_2, \dots, \varrho_k) & \mapsto & X_\varrho, \end{array}$$

where $S^k = [-\epsilon_1, \epsilon_1] \times [-\epsilon_2, \epsilon_2] \times \cdots \times [-\epsilon_k, \epsilon_k]$ with $\epsilon_i > 0$, $i = 1, 2, \dots, k$, sufficiently small.

In the next definition a half-open set U means either $U = V \cap \Sigma^+$ or $U = V \cap \Sigma^-$, where V is an open set in $\mathbb{R}^2$.

Definition 2.2. *We say that $W, \widetilde{W} \in \chi$ defined in half-open sets U and $\widetilde{U}$, respectively, are* C^0-orbitally equivalent *if there exists an orientation preserving homeomorphism $h : U \to \widetilde{U}$ that sends orbits of W to orbits of $\widetilde{W}$. Here, orbit of W means the image of a solution of $\dot{x} = W(x)$.*

Definition 2.3. *Two nonsmooth vector fields $Z = (X, Y)$, $\widetilde{Z} = (\widetilde{X}, \widetilde{Y}) \in \Omega$ defined in open sets U, $\widetilde{U}$ and with switching manifold Σ are* Σ-equivalent *if there exists an orientation preserving homeomorphism $h : U \to \widetilde{U}$ that sends $U \cap \Sigma$ to $\widetilde{U} \cap \Sigma$, the orbits of X restricted to $U \cap \Sigma^+$ to the orbits of $\widetilde{X}$ restricted to $\widetilde{U} \cap \Sigma^+$, and the orbits of Y restricted to $U \cap \Sigma^-$ to the orbits of $\widetilde{Y}$ restricted to $\widetilde{U} \cap \Sigma^-$.*

Consider the notation

$$X.f(p) = \langle \nabla f(p), X(p) \rangle \quad \text{and} \quad X^i.f(p) = \left\langle \nabla X^{i-1}.f(p), X(p) \right\rangle, \qquad i \geq 2,$$

where $\langle ., . \rangle$ is the usual inner product in $\mathbb{R}^2$.

Remark 2.4. *The vertical dotted lines in all figures of this paper that exhibit phase portraits represent the points $p \in V \subset \mathbb{R}^2$, where $X.f(p) = 0$ or $Y.f(p) = 0$.*

We distinguish the following regions on the discontinuity set Σ:

(i) $\Sigma^c \subseteq \Sigma$ is the *sewing region* if $(X.f)(Y.f) > 0$ on Σ^c.

(ii) $\Sigma^e \subseteq \Sigma$ is the *escaping region* if $(X.f) > 0$ and $(Y.f) < 0$ on Σ^e.

(iii) $\Sigma^s \subseteq \Sigma$ is the *sliding region* if $(X.f) < 0$ and $(Y.f) > 0$ on Σ^s.

Consider $Z \in \Omega$. The *sliding vector field* associated with Z is the vector field Z^s tangent to Σ^s and defined at $q \in \Sigma^s$ by $Z^s(q) = m - q$ with m being the point of the segment joining $q + X(q)$ and $q + Y(q)$ such that $m - q$ is tangent to Σ^s (see Figure 5). It is clear that if $q \in \Sigma^s$, then $q \in \Sigma^e$ for $-Z$, and then we can define the *escaping vector field* on Σ^e associated with Z by $Z^e = -(-Z)^s$. In what follows we use the notation Z^Σ for both cases. In our pictures we represent the dynamics of Z^Σ by double arrows.

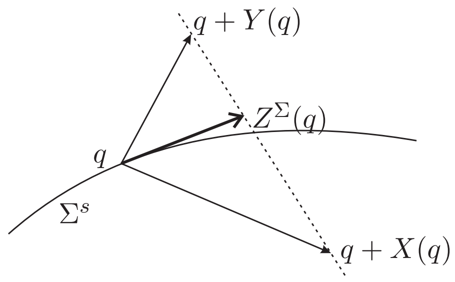

Figure 5. *Filippov's convention.*

Lemma 2.5. *Let $Z = (X, Y) \in \Omega$ present a fold-cusp singularity; then Z is Σ-equivalent to the standard form $Z_0 = Z_{\rho_1,\rho_2,\rho_3,\rho_4}$ given by*

$$Z_\rho = Z_{\rho_1,\rho_2,\rho_3,\rho_4} = \begin{cases} X_{\rho_1,\rho_2} = \begin{pmatrix} \rho_1 \\ \rho_2 x \end{pmatrix} & \text{if } y \geq 0, \\ Y_{\rho_3,\rho_4} = \begin{pmatrix} \rho_3 \\ \rho_4 x^2 \end{pmatrix} & \text{if } y \leq 0, \end{cases} \tag{2.1}$$

where $\rho_1, \rho_2, \rho_3, \rho_4 = \pm 1$.

Observe that the values of ρ_i, $i = 1, 2, 3, 4$, in Lemma 2.5 depend on the orientation of X and Y. In subsection 2.3 we prove Lemma 2.5; i.e., we exhibit the homeomorphism that characterizes the equivalence between any fold-cusp singularity and the standard form given by (2.1).

We say that $q \in \Sigma$ is a Σ-*regular point* if

(i) $(X.f(q))(Y.f(q)) > 0$ or

(ii) $(X.f(q))(Y.f(q)) < 0$ and $Z^\Sigma(q) \neq 0$ (that is, $q \in \Sigma^e \cup \Sigma^s$ and it is not an equilibrium point of Z^Σ).

The points of Σ which are not Σ-regular are called Σ-*singular*. We distinguish two subsets in the set of Σ-singular points: Σ^t and Σ^p. Any $q \in \Sigma^p$ is called a *pseudoequilibrium of* Z and is characterized by $Z^\Sigma(q) = 0$. Any $q \in \Sigma^t$ is called a *tangential singularity* and is characterized by $Z^\Sigma(q) \neq 0$ and $(X.f(q))(Y.f(q)) = 0$ (q is a contact point).

We say that a point $p_0 \in \Sigma$ is a Σ-*fold point* of X if $X.f(p_0) = 0$ but $X^2.f(p_0) \neq 0$. Moreover, $p_0 \in \Sigma$ is a *visible* (respectively, *invisible*) Σ-fold point of X if $X.f(p_0) = 0$ and $X^2.f(p_0) > 0$ (respectively, $X^2.f(p_0) < 0$). We say that a point $q_0 \in \Sigma$ is a Σ-*cusp point* of Y if $Y.f(q_0) = Y^2.f(q_0) = 0$ and $Y^3.f(q_0) \neq 0$. Moreover, a Σ-cusp point q_0 of Y is of *kind* 1 (respectively, *kind* 2) if $Y^3.f(q_0) > 0$ (respectively, $Y^3.f(q_0) < 0$). In particular, Σ-fold and Σ-cusp points are tangential singularities.

A pseudoequilibrium $q \in \Sigma^p$ is a Σ-*saddle* provided that one of the following conditions is satisfied: (i) $q \in \Sigma^e$ and q is an attractor for Z^Σ or (ii) $q \in \Sigma^s$ and q is a repeller for Z^Σ. A pseudoequilibrium $q \in \Sigma^p$ is a Σ-*repeller* (respectively, Σ-*attractor*) provided $q \in \Sigma^e$ (respectively, $q \in \Sigma^s$) and q is a repeller (respectively, attractor) equilibrium point for Z^Σ.

Given a point $q \in \Sigma^c$, we denote by $r(q)$ the straight line through $q + X(q)$ and $q + Y(q)$.

Definition 2.6. *The Σ-regular points $q \in \Sigma^c$ such that either $\{X(q), Y(q)\}$ is a linearly dependent set or $r(q) \cap \Sigma = \emptyset$ are called* virtual pseudoequilibria.

Let us consider a smooth autonomous vector field W defined in an open set U. Then we denote its flow by $\phi_W(t, p)$. Thus,

$$\begin{cases} \dfrac{d}{dt}\phi_W(t, p) = W(\phi_W(t, p)), \\ \phi_W(0, p) = p, \end{cases}$$

where $t \in I = I(p, W) \subset \mathbb{R}$, an interval depending on $p \in U$ and W.

The following definition was stated in [9, p. 1971].

Definition 2.7. *The* local trajectory *of an NSDS given by* (1.1) *is defined as follows:*

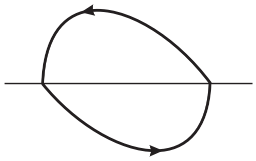

Figure 6. *Canard cycle of kind* I.

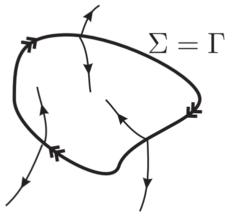

Figure 7. *Canard cycle of kind* II.

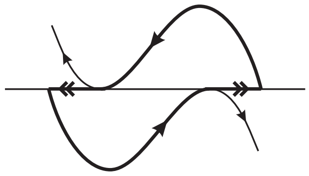

Figure 8. *Canard cycle of kind* III.

- *For $p \in \Sigma^+$ and $p \in \Sigma^-$ the trajectory is given by $\phi_Z(t,p) = \phi_X(t,p)$ and $\phi_Z(t,p) = \phi_Y(t,p)$, respectively, where $t \in I$.*
- *For $p \in \Sigma^c$ such that $X.f(p) > 0$, $Y.f(p) > 0$ and taking the origin of time at p, the trajectory is defined as $\phi_Z(t,p) = \phi_Y(t,p)$ for $t \in I \cap \{t \leq 0\}$, and $\phi_Z(t,p) = \phi_X(t,p)$ for $t \in I \cap \{t \geq 0\}$. For the case $X.f(p) < 0$ and $Y.f(p) < 0$ the definition is the same, reversing time.*
- *For $p \in \Sigma^e \cup \Sigma^s$ such that $Z^\Sigma(p) \neq 0$ we define $\phi_Z(t,p) = \phi_{Z^\Sigma}(t,p)$ for $t \in I$.*
- *For $p \in \partial\Sigma^c \cup \partial\Sigma^e \cup \partial\Sigma^s$ such that the definitions of trajectories for points in a full neighborhood of p in Σ can be extended to p and coincide, the trajectory through p is this trajectory.*
- *For any other point $\phi_Z(t,p) = p$ for all $t \in \mathbb{R}$. This is the case of points in $\partial\Sigma^c \cup \partial\Sigma^e \cup \partial\Sigma^s$ which are not regular tangential singularities and the equilibrium points of X in Σ^+, of Y in Σ^-, and of Z^Σ in $\Sigma^s \cup \Sigma^e$.*

Definition 2.8. *The* local orbit-arc *of the vector field W passing through a point $p \in U$ is the set $\gamma_W(p) = \{\phi_W(t,p) : t \in I\}$.*

Since we are dealing with autonomous systems, from now on we will use trajectory and orbit-arc indistinguishably when there is no danger of confusion.

Definition 2.9. *Consider $Z = (X,Y) \in \Omega$.*

1. *A* canard cycle *is a closed curve $\Gamma = \cup_{i=1}^n \sigma_i$ composed by the union of orbit-arcs σ_i, $i = 1, \dots, n$, of $X|_{\Sigma^+}$, $Y|_{\Sigma^-}$ and Z^Σ such that*
   - *either there exists $i_0 \subset \{1, \dots, n\}$ with $\sigma_{i_0} \subset \gamma_X$ (respectively, $\sigma_{i_0} \subset \gamma_Y$) and then there exists $j \neq i_0$ with $\sigma_j \subset \gamma_Y \cup \gamma_{Z^\Sigma}$ (respectively, $\sigma_j \subset \gamma_X \cup \gamma_{Z^\Sigma}$), or Γ is composed of a single arc σ_i of Z^Σ;*
   - *the transition between arcs of X and arcs of Y occurs in sewing points;*
   - *the transition between arcs of X (or Y) and arcs of Z^Σ occurs through Σ-fold points or regular points in the escaping or sliding arc, respecting the orientation. Moreover, if $\Gamma \neq \Sigma$, then there exists at least one visible Σ-fold point on each connected component of $\Gamma \cap \Sigma$.*
2. *A canard cycle Γ of Z is of*
   - Kind I *if Γ meets Σ just in sewing points;*
   - Kind II *if $\Gamma = \Sigma$;*
   - Kind III *if Γ contains at least one visible Σ-fold point of Z.*

   In Figures 6, 7, and 8 arise canard cycles of kinds I, II, *and* III, *respectively.*
3. *A canard cycle Γ of Z is* hyperbolic *if one of the following conditions is satisfied:*

(i) Γ *is of kind* I *and* $\eta'(p) \neq 1$, *where* η *is the first return map defined on a segment* T *with* $p \in T \pitchfork \gamma$;
(ii) Γ *is of kind* II;
(iii) Γ *is of kind* III, $\overline{\Sigma^e} \cap \overline{\Sigma^s} \cap \Gamma = \emptyset$, *and either* $\Gamma \cap \Sigma \subseteq \Sigma^c \cup \Sigma^e \cup \Sigma^t$ *or* $\Gamma \cap \Sigma \subseteq \Sigma^c \cup \Sigma^s \cup \Sigma^t$.

2.1. Global bifurcation. As said before, the configuration illustrated in Figure 4 plays a very important role in our analysis. The configuration of this figure is reached from (1.2) by taking $\beta > 0$, $\lambda = \sqrt{\beta}$, and $\mu = 0$. In this section we deal with this global phenomenon.

Let $Z_0 = (X_0, Y_0) \in \Omega$ having the following properties:

- Consider $X_0 = (f_1^0, g_1^0)$ and $Y_0 = (f_2^0, g_2^0)$ and assume that $f_1^0(p) > 0$ if $p \in \Sigma^+$ and $f_2^0(p) < 0$ if $p \in \Sigma^-$.
- $q_0 \in \Sigma$ is a visible Σ-fold point of Y_0 and $X.f(q_0) > 0$.
- The orbit $\gamma_{X_0}(q_0)$ of X_0 through q_0 meets Σ transversally at a point q_1.
- The orbit $\gamma_{Y_0}(q_1)$ of Y_0 through q_1 meets Σ tangentially at q_0. Call Γ the degenerate canard cycle composed by $\gamma_{X_0}(q_0)$ and $\gamma_{Y_0}(q_1)$. Let M be the compact region in the plane bounded by Γ.

2.1.1. Transition fold map. As $q_0 \in \Sigma$ is a visible Σ-fold point of Y_0, we may assume (see [15]) coordinates around q_0 such that the system is represented by $(\dot{x}, \dot{y}) = (-1, x)$ with $q_0 = (0, 0)$. The solutions of this differential equation are given by

$$\phi_{a,b}(t) = (-t + a, -(t^2/2) + at + b).$$

The orbit-arc ϕ_0 through $(0, 0)$ is represented by $\phi_0(t) = (-t, -t^2/2)$.

Let δ be a very small positive number. We construct the *transition map* $\xi : L_1 \to L_0$ from $L_1 = \{(x, y),\ y = -\delta,\ x \geq \sqrt{2\delta}\}$ to $L_0 = \{(x, 0),\ 0 \leq x \leq 2\sqrt{\beta}\}$, following the orbits of Y_0 (see Figure 9). The curve L_1 is transverse to Y_0 at $p_\delta = (\sqrt{2\delta}, -\delta)$. Since the solutions ϕ_δ through $(\overline{x}, -\delta) \in L_1$ meet $\Sigma = \{y = 0\}$ at time $t = \overline{x} \pm \sqrt{\overline{x}^2 - 2\delta}$ we obtain that $\xi(\overline{x}) = \sqrt{\overline{x}^2 - 2\delta}$ and ξ is an homeomorphism. Moreover, $\xi^{-1}(x) = \sqrt{x^2 + 2\delta}$, ξ^{-1} is differentiable at 0, and $(\xi^{-1})'(0) = 0$.

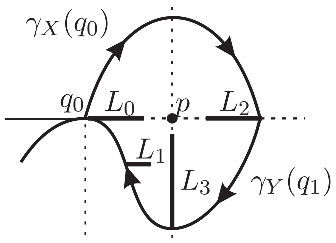

Figure 9. *First return map around the two-fold singularity* p.

2.1.2. First return map associated to Γ. Let ϱ_X be the transition map from L_0 to $L_2 = \{(x, 0),\ 2\sqrt{\beta} \leq x \leq 4\sqrt{\beta}\} \subset \Sigma$ via X_0-trajectories, and ϱ_Y be the transition map from L_2 to L_1 via Y_0-trajectories (see Figure 9). Observe that the linear part of the composition $\varrho_Y \circ \varrho_X$ is nonzero due to the transversality conditions of the problem. For simplicity, let $J_\epsilon = [0, \epsilon) \times \{0\}$ be a small semiopen interval of Σ.

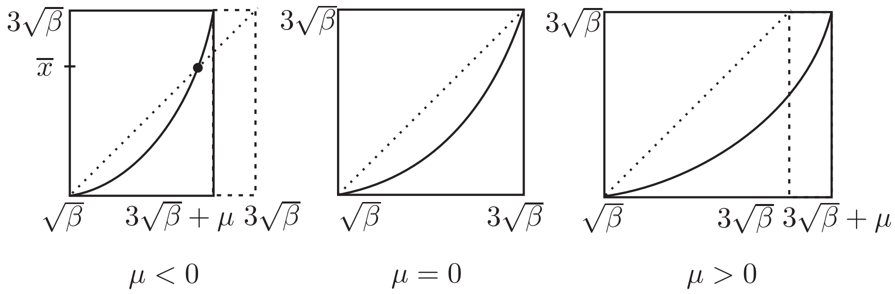

Figure 10. *Graph of the first return map* ψ_λ^μ.

So the first return map of Z_0 at q_0 is $\kappa(x)=(\xi\circ\varrho_Y\circ\varrho_X)(x)$ for $x\in J_\epsilon$. Its inverse κ^{-1} is a differentiable map at 0 and satisfies $(\kappa^{-1})'(0)=0$. So, Γ locally repels the orbits of Z_0 close to Γ and in the interior of Γ.

In conclusion, if Z is very close to Z_0 in Ω in such a way that it possesses a canard cycle nearby Γ, then it is a hyperbolic repeller canard cycle. Under some other conditions on Z_0 (reversing the directions of X_0 and Y_0) we can derive that such a canard cycle is an attractor.

2.1.3. Analysis around the two-fold singularity. In (1.2), for $\beta>0$, it is possible to define a *first return map* $\psi_\lambda^\mu:(\sqrt{\beta},3\sqrt{\beta}+\mu)\to(\sqrt{\beta},3\sqrt{\beta})$, associated to $Z_{\lambda,\beta,\mu}$, given by

$$\psi_\lambda^\mu(x)=(\varrho_{X_\lambda}\circ\varrho_{Y_{\mu,\beta}})(x),$$

where $\varrho_{Y_{\mu,\beta}}(x)$ is the first return to Σ of the orbit-arc of $Y_{\mu,\beta}$ that passes through $q=(x,0)$, and $\varrho_{X_\lambda}(\widetilde{x})$ is the first return to Σ of the orbit-arc of X_λ that passes through $\widetilde{q}=(\widetilde{x},0)$.

Lemma 2.10. *If $\beta>0$, $\lambda=\sqrt{\beta}$, and $\mu=0$ in (1.2), then (see Figure 4) the first return map $\psi_\lambda^\mu(x)$ satisfies*

(i) *$\psi_\lambda^0(x)<x$ for all $x\in(\sqrt{\beta},3\sqrt{\beta})$ and*

(ii) *$|(\psi_\lambda^0)'(\sqrt{\beta})|\neq1$.*

Proof. Consider Figure 4. Given a point $\overline{p}=(p_1,p_2)\in L_2$ (observe that $L_2=\{(x,0),\ \sqrt{\beta}\le x\le3\sqrt{\beta}\}$ in Figure 4), the positive Y-orbit through p reaches $L_3=\{(\sqrt{\beta},y),\ y\le0\}$ at the point $q=(q_1,q_2)$, and the negative X-orbit through p reaches L_0 at the point $\widetilde{p}=(\widetilde{p}_1,\widetilde{p}_2)$. The negative Y-orbit through $\widetilde{p}$ reaches L_3 at the point $\widetilde{q}=(\widetilde{q}_1,\widetilde{q}_2)$. Since

$$q_2-\widetilde{q}_2=\frac{(p_1-3\sqrt{\beta})(p_1-\sqrt{\beta})^3\Big(p_1(1744+99\sqrt{\beta})-\sqrt{\beta}(6256+321\beta)\Big)}{384\beta}$$

and $\sqrt{\beta}<p_1<3\sqrt{\beta}$ we conclude that $q_2-\widetilde{q}_2>0$, and item (i) is proved. Item (ii) follows from section 2.1.2. ∎

Note that Lemma 2.10 implies that $Z_{\sqrt{\beta},\beta,0}$ does not have closed orbits in the interior of the closed orbit of Z passing through the visible Σ-fold point of $Y_{0,\beta}$. Moreover, when $\mu<0$ (see Figure 10), Lemma 2.10 guarantees that ψ_λ^μ has a unique fixed point $\overline{x}$, where $\overline{x}<3\sqrt{(\beta)}+\mu$. And, in this case, $|(\psi_\lambda^\mu)'(\overline{x}))|\neq1$; i.e., $\overline{x}$ is a hyperbolic fixed point for ψ_λ^μ that corresponds to a hyperbolic canard cycle of $Z_{\lambda,\beta,\mu}$. When $\mu>0$ (see Figure 10), $\psi_\lambda^\mu(x)<x$ for all $x\in(\sqrt{\beta},3\sqrt{\beta}+\mu)$, and closed orbits of $Z_{\lambda,\beta,\mu}$ do not arise.

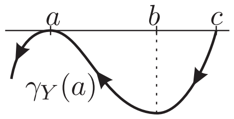

Figure 11. *Case Y^+.*

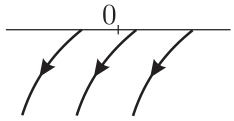

Figure 12. *Case Y^-.*

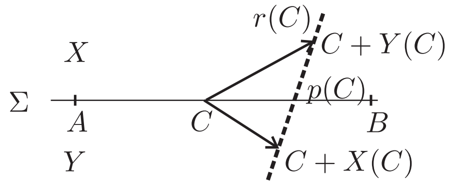

Figure 13. *Direction function.*

Given $Z=(X,Y)$, we describe some properties of both $X=X_\lambda$ and either $Y=Y_{\beta,\mu}$ or $Y=Y_\beta$.

The parameter λ measures how the Σ-fold point $d=(\lambda,0)$ of X is translated away from the origin. More specifically, if $\lambda<0$, then d is translated to the left-hand side, and if $\lambda>0$, then d is translated to the right-hand side.

The parameter β distinguishes the contact order between a trajectory of Y and Σ. In this way, there occurs one, and only one, of the following situations:

- $\mathbf{Y^+}$: In this case $\beta>0$. So Y has two Σ-fold points in such a way that one of them is invisible and the other one is visible. These points are expressed by $a=a_\beta=(-\sqrt{\beta},0)$ and $b=b_\beta=(\sqrt{\beta},0)$. Moreover, a third point $c=c_{\beta,\mu}=(3\sqrt{\beta}+\mu,0)$ plays an important role in the analysis of (1.2). This point is the locus where the orbit-arc $\gamma_Y(a)$ intersects Σ transversally for negative time (see Figure 11). Using the bump function B, the distance between c and b is bigger or smaller than the distance between a and b according to the value of the parameter μ. This fact will be important to change from Theorem 1 to Theorems 2 and 3.
- $\mathbf{Y^0}$: In this case $\beta=0$. So Y has a Σ-cusp point $e=(0,0)$ (see Figure 1).
- $\mathbf{Y^-}$: In this case $\beta<0$. So Y does not have Σ-fold points. In this way, $Y.f\neq 0$, and Y is transversal to Σ (see Figure 12).

2.2. The direction function. The next function will be very useful in what follows.

On Σ, consider the point $C=(C_1,C_2)$ and the vectors $X(C)=(D_1,D_2)$ and $Y(C)=(E_1,E_2)$ (as illustrated in Figure 13). Observe that the straight line $r(C)$ by $q+X(q)$ and $q+Y(q)$, generically, meets Σ in a point $p(C)$. We define the C^r-map

$$\begin{array}{rccc} p: & \Sigma & \longrightarrow & \Sigma, \\ & z & \longmapsto & p(z). \end{array}$$

We choose local coordinates such that Σ is the x-axis; so $C=(C_1,0)$ and $p(C)\in\mathbb{R}\times\{0\}$ can be identified with points in $\mathbb{R}$. According with this identification, the *direction function* on Σ is defined by

$$\begin{array}{rccc} H: & \mathbb{R} & \longrightarrow & \mathbb{R}, \\ & z & \longmapsto & p(z)-z. \end{array}$$

Remark 2.11. *We obtain that H is a C^r-map. When $C \in \Sigma^e \cup \Sigma^s$ the following holds:*

- *if $H(C) < 0$, then the orientation of Z^Σ in a small neighborhood of C is from B to A;*
- *if $H(C) = 0$, then $C \in \Sigma^p$;*
- *if $H(C) > 0$, then the orientation of Z^Σ in a small neighborhood of C is from A to B.*

Simple calculations show that $p(C_1) = \frac{E_2(D_1+C_1)-D_2(E_1+C_1)}{E_2-D_2}$, and consequently,

$$H(C_1) = \frac{E_2 D_1 - D_2 E_1}{E_2 - D_2}. \tag{2.2}$$

Remark 2.12. *If $X.f(p) = 0$ and $Y.f(p) \neq 0$, then, in a neighborhood V_p of p in Σ, we have $H(V_p)D_1 > 0$, where $X(p) = (D_1, D_2)$. In fact, $X.f(p) = 0$ and $Y.f(p) \neq 0$ are equivalent to saying that $D_2 = 0$ and $E_2 \neq 0$ in (2.2). So, $\lim_{(D_2,E_2)\to(0,k_0)} H(p_1) = D_1$, where $k_0 \neq 0$ and $p = (p_1, p_2)$.*

Considering the previous notation and identifying Σ with the x-axis, we have that $r(C) \cap \Sigma = \emptyset$ when $E_2 = D_2$. In such a case, H is not defined at C. The following property is immediate.

Proposition 2.13. *If n_1 is the number of pseudoequilibria and n_2 is the number of virtual pseudoequilibria, then $n_1 + n_2 = v_1 + v_2$, where v_1 is the number of zeros of H and v_2 is the number of points q of Σ such that $r(q) \cap \Sigma = \emptyset$.*

Proof. The proof is straightforward according to Remark 2.11, (2.2), and Definition 2.6. ■

Remark 2.14. *Given $Z_{\lambda,\beta,\mu}$, we list some properties of the function H. According to (2.2) we have that the expression of H is*

$$H(x, \lambda, \beta, \mu) = \frac{H_1(x, \lambda, \beta, \mu)}{H_2(x, \lambda, \beta, \mu)},$$

where $H_1(x, \lambda, \beta, \mu) = -x^2 - x + \lambda + \beta - \frac{\partial B}{\partial x}(x, \beta, \mu)$ and $H_2(x, \lambda, \beta, \mu) = -x^2 + x - \lambda + \beta - \frac{\partial B}{\partial x}(x, \beta, \mu)$. So,

(i) *When $x = \lambda$ we get $H_1(\lambda, \lambda, \beta, \mu) = H_2(\lambda, \lambda, \beta, \mu)$.*

(ii) *For the parameter values satisfying $\beta = \lambda^2 + \frac{\partial B}{\partial x}(\lambda, \beta, \mu) > 0$ we have $H_1(\lambda, \lambda, \beta, \mu) = H_2(\lambda, \lambda, \beta, \mu) = 0$.*

(iii) *Since $H_1(0, 0, 0, 0) = 0$ (respectively, $H_2(0, 0, 0, 0) = 0$) and $\frac{\partial H_1}{\partial x}(0, 0, 0, 0) = -1$ (respectively, $\frac{\partial H_2}{\partial x}(0, 0, 0, 0) = 1$), by the implicit function theorem there is a unique $x = x_{H_1}(\lambda, \beta, \mu)$ such that $H_1(x_{H_1}(\lambda, \beta, \mu), \lambda, \beta, \mu) = 0$ (respectively, $H_2(x_{H_2}(\lambda, \beta, \mu), \lambda, \beta, \mu) = 0$). Therefore, there is only one zero of H_1 and only one zero of H_2 in a sufficiently small neighborhood of $x = 0$. These points are called p_1 and r_1, respectively, in Figure 14. The pseudoequilibrium p_1 and the virtual pseudoequilibrium r_1 are the unique roots of H_1 and H_2, respectively, that are relevant to our analysis. In fact, the other roots are far from the origin.*

2.3. Proof of Lemma 2.5.

Here we construct a Σ-preserving homeomorphism h that sends orbits of $Z = (X, Y)$ to orbits of $\widetilde{Z} = (\widetilde{X}, \widetilde{Y})$, where $\widetilde{Z} = Z_\rho$ is given by (2.1) with $\rho_1 = 1$ and $\rho_i = -1$, $i = 2, 3, 4$. The other choices on parameters ρ_i, $i = 1, 2, 3, 4$, are treated in a similar way. Let p (respectively, $\widetilde{p}$) be the fold-cusp singularity of Z (respectively, $\widetilde{Z}$) (see

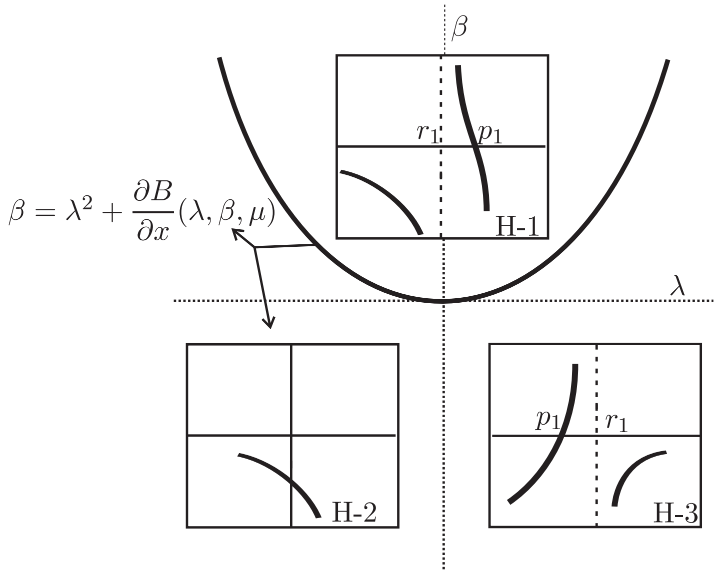

Figure 14. *Variation of H with respect to λ and β. The dark lines in the boxes* H-1, H-2, *and* H-3 *correspond to the graph of H.*

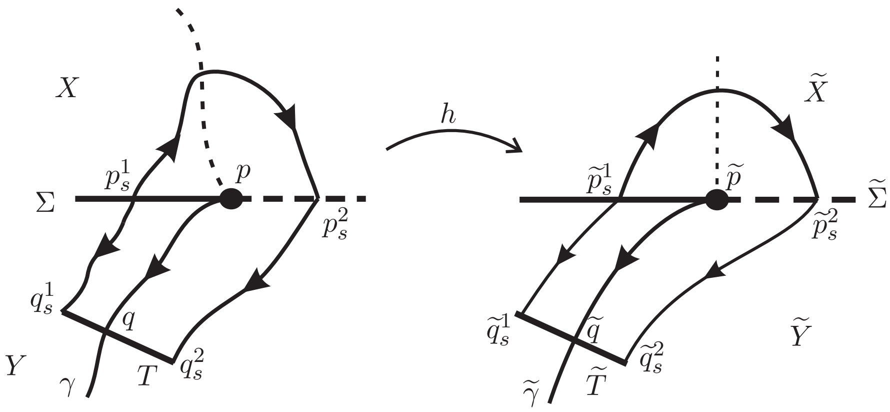

Figure 15. *Construction of the homeomorphism.*

Figure 15). Identify p with $\widetilde{p}$; i.e., $h(p) = \widetilde{p}$. Consider a point $q \in \gamma$ (respectively, $\widetilde{q} \in \widetilde{\gamma}$), where γ (respectively, $\widetilde{\gamma}$) is the orbit-arc of Y (respectively, $\widetilde{Y}$) starting at p (respectively, $\widetilde{p}$). Identify γ with $\widetilde{\gamma}$ (i.e., $h(\gamma) = \widetilde{\gamma}$) from a reparametrization by arc-length. Let T (respectively, $\widetilde{T}$) be transversal sections to Y (respectively, $\widetilde{Y}$) passing through q (respectively, $\widetilde{q}$) with small amplitude. Identify T with $\widetilde{T}$ (i.e., $h(T) = \widetilde{T}$) by arc-length. Let $q_s^1 \in T$ be a point on the left of q. Using the implicit function theorem (abbreviated by IFT), there exists a time $t_s^1 < 0$, depending on q_s^1, such that $\phi_Y(q_s^1, t_s^1) := p_s^1 \in \Sigma$. Since $h(T) = \widetilde{T}$, there exists $\widetilde{q}_s^1 \in \widetilde{T}$ such that $h(q_s^1) = \widetilde{q}_s^1$. Using the IFT, there exists a time $\widetilde{t}_s^1 < 0$, depending on $\widetilde{q}_s^1$, such that $\phi_{\widetilde{Y}}(\widetilde{q}_s^1, \widetilde{t}_s^1) := \widetilde{p}_s^1 \in \widetilde{\Sigma}$. Identify the orbit-arc $\sigma_{q_s^1}^{p_s^1}(Y)$ of Y joining p_s^1 to q_s^1 with the orbit-arc $\widetilde{\sigma}_{\widetilde{q_s^1}}^{\widetilde{p_s^1}}(\widetilde{Y})$ of $\widetilde{Y}$ joining $\widetilde{p}_s^1$ to $\widetilde{q}_s^1$ (i.e., $h(\sigma_{q_s^1}^{p_s^1}(Y)) = \widetilde{\sigma}_{\widetilde{q_s^1}}^{\widetilde{p_s^1}}(\widetilde{Y})$) by arc-length. Fix the notation for the orbit-arcs of a given vector field joining two points. Since p (respectively, $\widetilde{p}$) is a Σ-fold point of X (respectively, $\widetilde{X}$), using the IFT, there exists a time $t_s^2 > 0$ (respectively, $\widetilde{t}_s^2 > 0$), depending on p_s^1 (respectively, $\widetilde{p}_s^1$), such that $\phi_X(p_s^1, t_s^2) := p_s^2 \in \Sigma$ (respectively, $\phi_{\widetilde{X}}(\widetilde{p}_s^1, \widetilde{t}_s^2) := \widetilde{p}_s^2 \in \widetilde{\Sigma}$). Identify $\sigma_{p_s^1}^{p_s^2}(X)$ with $\widetilde{\sigma}_{\widetilde{p_s^1}}^{\widetilde{p_s^2}}(\widetilde{X})$ (i.e., $h(\sigma_{p_s^1}^{p_s^2}(X)) = \widetilde{\sigma}_{\widetilde{p_s^1}}^{\widetilde{p_s^2}}(\widetilde{X})$) by arc-length. Using the IFT, there exists a time $t_s^3 > 0$ (respectively, $\widetilde{t}_s^3 > 0$), depending on p_s^2 (respectively, $\widetilde{p}_s^2$), such that $\phi_Y(p_s^2, t_s^3) := q_s^2 \in T$ (respectively, $\phi_{\widetilde{Y}}(\widetilde{p}_s^2, \widetilde{t}_s^3) := \widetilde{q}_s^2 \in \widetilde{T}$). Identify $\sigma_{p_s^2}^{q_s^2}(Y)$ with $\widetilde{\sigma}_{\widetilde{p_s^2}}^{\widetilde{q_s^2}}(\widetilde{Y})$ (i.e., $h(\sigma_{p_s^2}^{q_s^2}(Y)) = \widetilde{\sigma}_{\widetilde{p_s^2}}^{\widetilde{q_s^2}}(\widetilde{Y})$) by arc-length.

So, the homeomorphism h sends Σ to $\widetilde{\Sigma}$ and sends orbits of Z to orbits of $\widetilde{Z}$. ■

3. Proof of Theorem 1. In Case 1_1 we assume that Y presents the behavior Y^-, where $\beta < 0$. In Cases 2_1, 3_1, and 4_1 we assume that Y presents the behavior Y^0, where $\beta = 0$. In these cases canard cycles do not arise (for a proof, see [4]).

◇ *Case* 1_1: $\beta < 0$. The points of Σ on the left of d belong to Σ^e, and the points on the right of d belong to Σ^c. See Figure 16. Since $\beta < 0$, the graph of H is illustrated in H-3 of Figure 14. We get that $p_1 = (-1 + \sqrt{1 + 4\beta + 4\lambda}/2, 0) \in \Sigma^e$ is a Σ-repeller and $r_1 = (1 - \sqrt{1 + 4\beta - 4\lambda}/2, 0) \in \Sigma^c$.

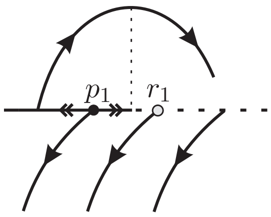

Figure 16. *Case* 1_1.

◇ *Case* 2_1: $\lambda < 0$, *Case* 3_1: $\lambda = 0$, *and Case* 4_1: $\lambda > 0$. The configuration of the connected components of Σ is the same as in Case 1_1. Since $\beta = 0$, the graph of H, when $\lambda \neq 0$, is given by H-3 of Figure 14. When $\lambda = 0$ (Case 3_1), the graph of H is given by H-2 of Figure 14 and $p_1 = r_1$. These cases are illustrated in Figure 17.

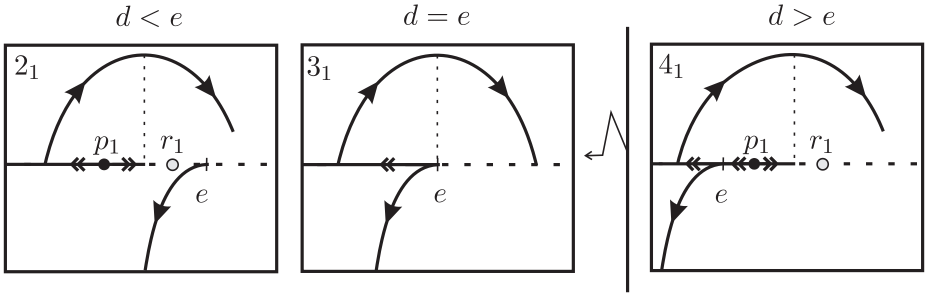

Figure 17. *Cases* 2_1, 3_1, *and* 4_1.

In Cases 5_1–17_1 we assume that Y presents the behavior Y^+, where $\beta > 0$.

⋄ *Case* 5_1: $\lambda < -\sqrt{\beta}$. The points of Σ on the left of d belong to Σ^e, the points inside the interval (a, b) belong to Σ^s, and the points on (d, a) and on the right of b belong to Σ^c. The graph of H is like H-3 of Figure 14. We can prove that p_1 is a Σ-repeller situated on the left of d and $r_1 \in (d, a)$. Canard cycles do not arise. See Figure 18.

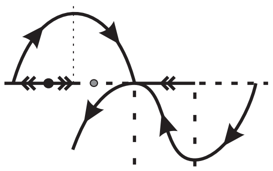

Figure 18. *Case* 5_1.

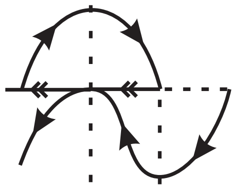

Figure 19. *Case* 6_1.

⋄ *Case* 6_1: $\lambda = -\sqrt{\beta}$. In this case the points on the right of b belong to Σ^c, the points on $(a = d, b)$ belong to Σ^s, and the points on the left of $a = d$ belong to Σ^e. Since $\beta = \lambda^2$, H is like H-2 of Figure 14 and $p_1 = r_1$. There exists a nonhyperbolic canard cycle Γ of kind III passing through a and c. See Figure 19.

⋄ *Case* 7_1: $-\sqrt{\beta} < \lambda < 0$, *Case* 8_1: $\lambda = 0$, *and Case* 9_1: $0 < \lambda < \sqrt{\beta}$. The configuration of the connected components of Σ is like Case 5_1, replacing a by d and vice versa. The graph of H is like H-1 of Figure 14. We observe that $p_1 \in (d, b)$ is a Σ-attractor and $r_1 \in (a, d)$. There exists a hyperbolic repeller canard cycle Γ of kind III passing through a and c. See Figure 20.

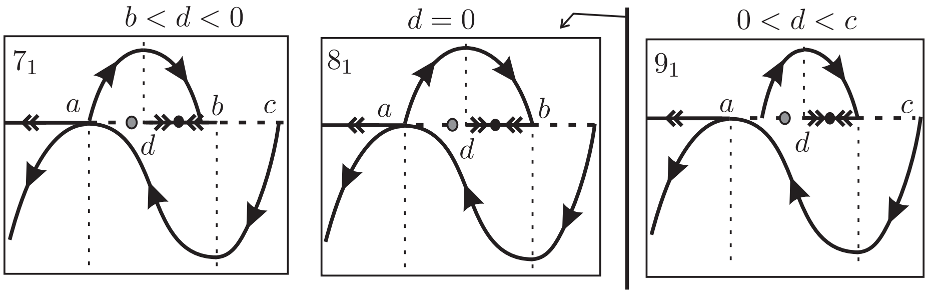

Figure 20. *Cases* 7_1–9_1.

⋄ *Case* 10_1: $\lambda = \sqrt{\beta}$. In this case the points on the left of a belong to Σ^e, and the points on the right of a belong to Σ^c, except by $Q = (b, 0) \in \Sigma$. Since $\beta = \lambda^2$, H is like H-2 of Figure 14 and $p_1 = r_1$. Since $\mu = 0$ and $d = b$, by the construction of the bump function B it is straightforward to show that the point Q behaves itself like a weak attractor for Z and there exists a nonhyperbolic canard cycle of kind III passing through a and c. See Figure 4. This case has already been discussed previously in subsection 2.1. Note that in [9] the authors avoid this case.

⋄ *Case* 11_1: $\sqrt{\beta} < \lambda < L_1$. The meaning of the value L_1 will be given below in this case. The points of Σ on the left of a and on (b, d) belong to Σ^e. The points on (a, b) and on the right of d belong to Σ^c. The graph of H is like H-3 of Figure 14. We can prove that $p_1 \in (b, d)$

is a Σ-repeller and r_1 is on the right of d. Since the point Q of the previous case is a weak attractor, in a neighborhood of d there occurs a *Hopf-like bifurcation.* Moreover, according to Lemma 2.10, there is a unique canard cycle Γ_1 in a neighborhood of d and a unique canard cycle Γ_2 in a neighborhood of c. Observe that both are of kind I, Γ_1 is attractor, Γ_2 is repeller, and Γ_1 is located within the region bounded by Γ_2. See Figure 21. Note that, as λ increases, Γ_1 becomes bigger and Γ_2 becomes smaller. When λ assumes the limit value L_1, one of them collides with the other.

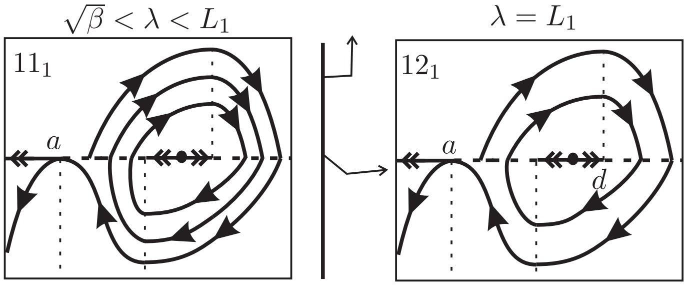

Figure 21. *Cases* 11_1 *and* 12_1.

$\diamond$ *Case* 12_1: $\lambda = L_1$. The distribution of the connected components of Σ and the behavior of H are the same as in Case 11_1. Since $\lambda = L_1$, as described in the previous case, there exists a nonhyperbolic canard cycle Γ of kind I which is an attractor for the trajectories inside it and is a repeller for the trajectories outside it. See Figure 21.

$\diamond$ *Case* 13_1: $L_1 < \lambda < 2\sqrt{\beta}$, *Case* 14_1: $\lambda = 2\sqrt{\beta}$, *Case* 15_1: $2\sqrt{\beta} < \lambda < 3\sqrt{\beta}$, *Case* 16_1: $\lambda = 3\sqrt{\beta}$, *and Case* 17_1: $\lambda > 3\sqrt{\beta}$. The distribution of the connected components of Σ and the behavior of H are the same as in Case 11_1. Canard cycles do not arise. See Figure 22.

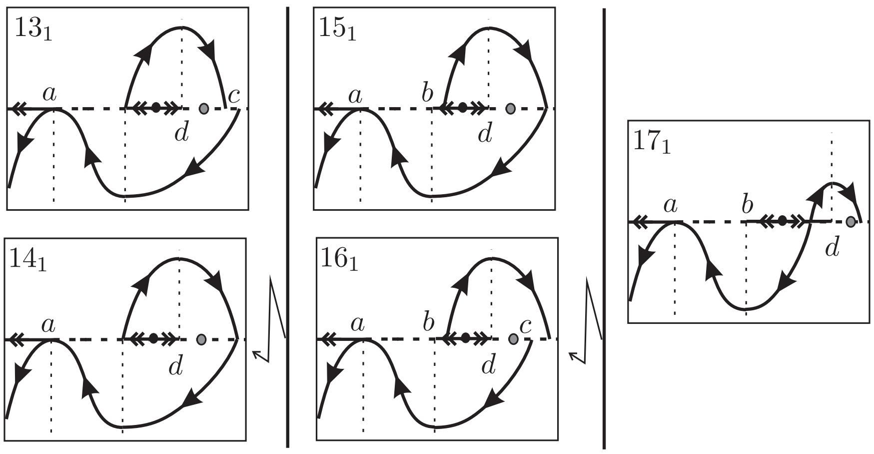

Figure 22. *Cases* 13_1–17_1.

The bifurcation diagram is illustrated in Figure 23. ■

Remark 3.1. *In Cases* 9_1 *and* 11_1 *the ST-bifurcations (as described in* [9, subsections 11.2 and 12.2]*) arise. In fact, note that the trajectory passing through* a *in Case* 9_1*, and* c *in Case*

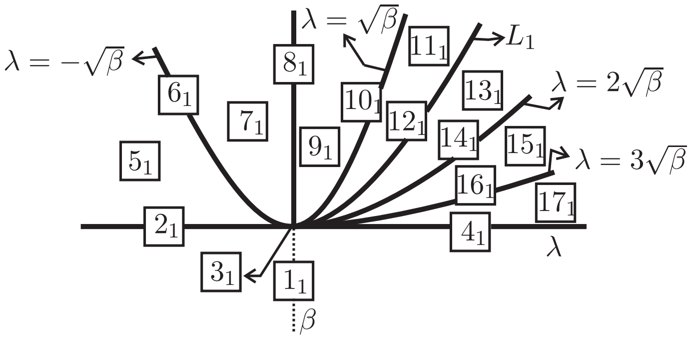

Figure 23. *Bifurcation diagram of Theorem 1.*

11_1, *can make more and more turns around* p_1. *This fact characterizes a global bifurcation also reached in other cases.*

4. Proof of Theorem 2.

In Case 1_2 we assume that Y presents the behavior Y^-. In Cases 2_2, 3_2, and 4_2 we assume that Y presents the behavior Y^0. In Cases 5_2–19_2 we assume that Y presents the behavior Y^+.

⋄ *Case* 1_2: $\beta < 0$, *Case* 2_2: $\lambda < 0$, *Case* 3_2: $\lambda = 0$, *Case* 4_2: $\lambda > 0$, *Case* 5_2: $\lambda < -\sqrt{\beta}$, *Case* 6_2: $\lambda = -\sqrt{\beta}$, *Case* 7_2: $-\sqrt{\beta} < \lambda < 0$, *and Case* 8_2: $\lambda = 0$. By the choice of the bump function B, these cases are analogous to Cases 1_1, 2_1, 3_1, 4_1, 5_1, 6_1, 7_1, and 8_1.

⋄ *Case* 9_2: $0 < \lambda < \sqrt{\beta} - \mu/2$. The analysis of this case is done in a similar way as for Case 9_1. In this case and in Cases 7_2 and 8_2 there exists a hyperbolic repeller canard cycle Γ of kind III passing through a and c.

⋄ *Case* 10_2: $\lambda = \sqrt{\beta} - \mu/2$. The points of Σ on the left of a belong to Σ^e, and the points on (d, b) belong to Σ^s. The points on (a, d) and on the right of b belong to Σ^c. The graph of H is like H-3 of Figure 14. Observe that $p_1 \in (d, b)$ is a Σ-attractor, and r_1 is on the right of b. In this case the arc $\gamma_X(a)$ of X passing through a returns to Σ at the point c. So, in this case there arises a nonhyperbolic canard cycle $\Gamma = \gamma_X(a) \cup \gamma_Y(c)$. By the discussion on subsection 2.1.2, we have that Γ is a repeller and we do not have other canard cycles inside Γ. See Figure 24.

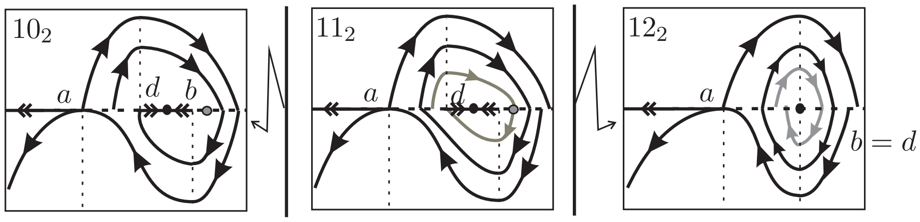

Figure 24. *Cases* 10_2–12_2.

⋄ *Case* 11_2: $\sqrt{\beta} - \mu/2 < \lambda < \sqrt{\beta}$. The configuration on Σ and the graph of H are the same as in Case 10_2. Since $\varrho_X^{-1}(c) \in (a, d)$ there exists a point $Q \in (\varrho_X^{-1}(c), \varrho_X^{-1}(b))$ such that $\eta'(Q) = 1$. So there exists a hyperbolic repeller canard cycle Γ, of kind I, passing through

Q. See Figure 24. Moreover, by Lemma 2.10 this canard cycle is unique. In Figure 10 we introduced the point $\overline{x}$ which plays the same role of Q.

⋄ *Case* 12_2: $\lambda = \sqrt{\beta}$. The points of Σ on the left of a belong to Σ^e, and the points on the right of a belong to Σ^c, except by the tangential singularity $c = d$. The graph of H is like H-2 of Figure 14. The repeller canard cycle Γ presented in the previous case is persistent. Recall that this canard cycle is born from the bifurcation of Case 10_2. So, the radius of Γ does not tend to zero when λ tends to $\sqrt{\beta}$. Moreover, the tangential singularity $b = d$ behaves itself like a weak attractor. See Figure 24.

⋄ *Case* 13_2: $\sqrt{\beta} < \lambda < L_1$, *Case* 14_2: $\lambda = L_1$, *Case* 15_2: $L_1 < \lambda < 2\sqrt{\beta} + \mu/2$, *Case* 16_2: $\lambda = 2\sqrt{\beta} + \mu/2$, *Case* 17_2: $2\sqrt{\beta} + \mu/2 < \lambda < 3\sqrt{\beta} + \mu$, *Case* 18_2: $\lambda = 3\sqrt{\beta} + \mu$, *and Case* 19_2: $\lambda > 3\sqrt{\beta} + \mu$. The analysis of these cases is done in a similar way as for Cases 11_1, 12_1, 13_1, 14_1, 15_1, 16_1, and 17_1, respectively.

The bifurcation diagram is illustrated in Figure 25. ■

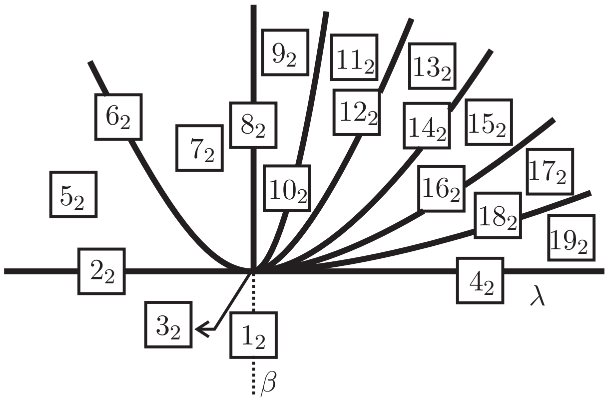

Figure 25. *Bifurcation diagram of Theorems 2 and 3.*

5. Proof of Theorem 3.

In Case 1_3 we assume that Y presents the behavior Y^-. In Cases 2_3, 3_3, and 4_3 we assume that Y presents the behavior Y^0. In Cases 5_3–19_3 we assume that Y presents the behavior Y^+.

⋄ *Case* 1_3: $\beta < 0$, *Case* 2_3: $\lambda < 0$, *Case* 3_3: $\lambda = 0$, *Case* 4_3: $\lambda > 0$, *Case* 5_3: $\lambda < -\sqrt{\beta}$, *Case* 6_3: $\lambda = -\sqrt{\beta}$, *Case* 7_3: $-\sqrt{\beta} < \lambda < 0$, *Case* 8_3: $\lambda = 0$, *and Case* 9_3: $0 < \lambda < \sqrt{\beta}$. By the choice of the bump function B, these cases are analogous to Cases 1_1, 2_1, 3_1, 4_1, 5_1, 6_1, 7_1, 8_1, and 9_1.

⋄ *Case* 10_3: $\lambda = \sqrt{\beta}$. The distribution of the connected components of Σ and the behavior of H are the same as in Case 12_2. This case differs from Case 12_2 because, as observed in subsection 2.1.3, when $\lambda = \sqrt{\beta}$ and $\mu > 0$ canard cycles of Z do not arise (see Figure 10) bifurcating from the nonhyperbolic canard cycle Γ of Case 12_3 below. Moreover, the tangential singularity $d = b$ behaves itself like a weak attractor. See Figure 26. There exists a hyperbolic repeller canard cycle Γ of kind III passing through a and c.

⋄ *Case* 11_3: $\sqrt{\beta} < \lambda < \sqrt{\beta} - \mu/2$. The points of Σ on the left of a and on (b, d) belong to Σ^e. The points on (a, b) and on the right of d belong to Σ^c. The graph of H is like H-3 of Figure 14. We can prove that $p_1 \in (b, d)$ is a Σ-repeller and r_1 is on the right of d. Since

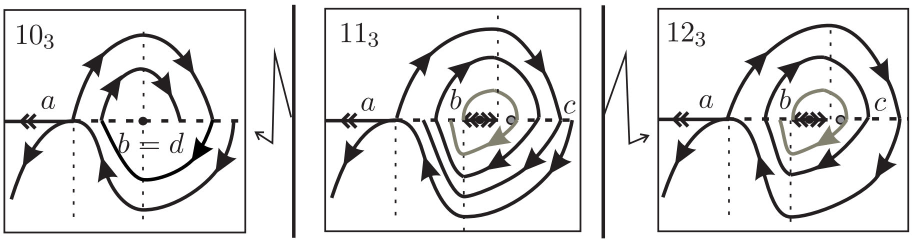

Figure 26. *Cases* 10_3–12_3.

$\varrho_Y(\varrho_X(a)) \in (a,b)$ there exists a point $Q \in (\varrho_Y(\varrho_X(a)), \varrho_Y(d))$ such that $\eta'(Q) = 1$. So there exists a hyperbolic attractor canard cycle Γ, of kind I, passing through Q. See Figure 26. By Lemma 2.10, in this Hopf bifurcation a unique canard cycle arises. Moreover, there exists a hyperbolic repeller canard cycle Γ of kind III passing through a and c.

⋄ *Case* 12_3: $\lambda = \sqrt{\beta} - \mu/2$. The configuration on Σ and the graph of H are the same as in Case 11_3. The attractor canard cycle Γ presented in the previous case is persistent. Recall that this canard cycle is born from the bifurcation of Case 10_3. So, the radius of Γ does not tend to zero when λ tends to $\sqrt{\beta}+\mu/2$. Moreover, it appears as a nonhyperbolic canard cycle passing through a and c. See Figure 26.

⋄ *Case* 13_3: $\sqrt{\beta} - \mu/2 < \lambda < L_1$, *Case* 14_3: $\lambda = L_1$, *Case* 15_3: $L_1 < \lambda < 2\sqrt{\beta} - \mu/2$, *Case* 16_3: $\lambda = 2\sqrt{\beta} - \mu/2$, *Case* 17_3: $2\sqrt{\beta} - \mu/2 < \lambda < 3\sqrt{\beta} - \mu$, *Case* 18_3: $\lambda = 3\sqrt{\beta} - \mu$, *and Case* 19_3: $\lambda > 3\sqrt{\beta} - \mu$. The analysis of these cases is done in a similar way as for Cases 11_1, 12_1, 13_1, 14_1, 15_1, 16_1, and 17_1, respectively.

The bifurcation diagram is illustrated in Figure 25, replacing the number 2 subscript by the number 3. ∎

6. Proof of Theorem A.

Since in (1.2) we can take $\mu \in (-\mu_0, \mu_0)$, from Theorems 1, 2, and 3 we derive that its bifurcation diagram contains all the 55 cases described in Theorems 1, 2, and 3. However, some of them are Σ-equivalent, and the number of distinct topological behaviors is 23. Moreover, each topological behavior can be represented respectively by the Cases 1_1, 2_1, 3_1, 4_1, 5_1, 6_1, 7_1, 8_1, 9_1, 10_1, 11_1, 12_1, 13_1, 14_1, 15_1, 16_1, 17_1, 10_2, 11_2, 12_2, 10_3, 11_3, and 12_3.

The full behavior of the 3-parameter family of NSDSs expressed by (1.2) is illustrated in Figure 27, where we consider a sphere around the point $(\lambda, \beta, \mu) = (0,0,0)$ with a small ray, and so we make a stereographic projection defined on the entire sphere except the south pole. Still, in relation to this figure, the numbers pictured correspond to the occurrence of the cases described in the previous theorems. As expected, Cases 3_1 and 3_2 are not represented in this figure because they are, respectively, the center and the south pole of the sphere. ∎

7. Proof of Theorem B.

When we consider (1.4), the function H, given by (2.2), is constant and equal to 1 independent of the value of μ. Moreover, distinct values of the bump function $\widetilde{B}$ (where $\widetilde{B} \neq B$) do not produce any topological change in the bifurcation diagram of the singularity. In other words, two parameters are enough to describe the full behavior of this singularity. Observe that, by Proposition 2.13, we have $\Sigma^f = \emptyset$, and it does not have virtual pseudoequilibria.

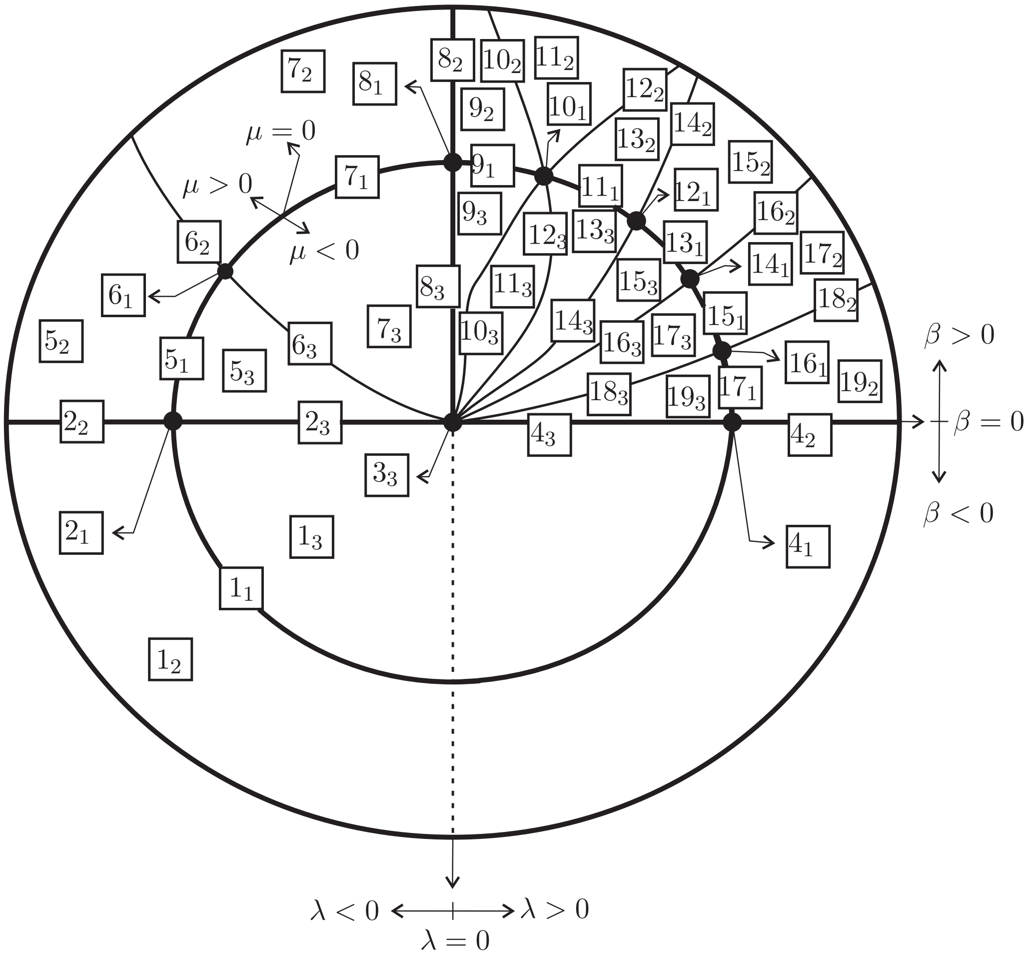

Figure 27. *Bifurcation diagram of the invisible fold-cusp singularity.*

Since X has a unique Σ-fold point which is visible, we conclude that canard cycles do not arise. In Case 1_B we assume that Y presents the behavior Y^-. In Cases 2_B, 3_B, and 4_B we assume that Y presents the behavior Y^0. In Cases 5_B–11_B we assume that Y presents the behavior Y^+.

$\diamond$ *Case* 1_B: $\beta < 0$. The points of Σ on the left of d belong to Σ^c, and the points on the right of d belong to Σ^e. See Figure 28.

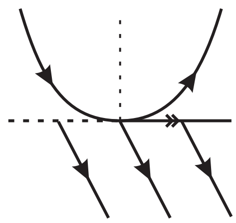

Figure 28. *Case* 1_B.

$\diamond$ *Case* 2_B: $\lambda < 0$, *Case* 3_B: $\lambda = 0$, *and Case* 4_B: $\lambda > 0$. The configuration of the connected components of Σ is the same as in Case 1_B. Note that, when $\lambda < 0$ (Case 2_B), it appears a tangential singularity $P = (\lambda, 0) \in \Sigma^e$, but Z^Σ is always oriented from the left to the right. These cases are illustrated in Figure 29.

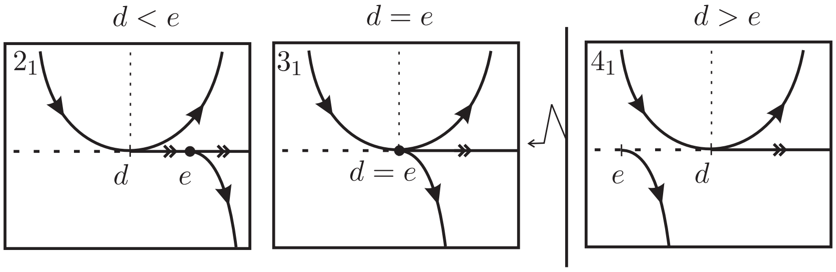

Figure 29. *Cases* 2_B*–*4_B*.*

$\diamond$ *Case* 5_B: $\lambda < -2\sqrt{\beta}$, *Case* 6_B: $\lambda = -2\sqrt{\beta}$, *and Case* 7_B: $-2\sqrt{\beta} < \lambda < -\sqrt{\beta}$. The points of Σ on the right of b and inside the interval (d, a) belong to Σ^e. The points on (a, b) and on the left of d belong to Σ^c. See Figure 30.

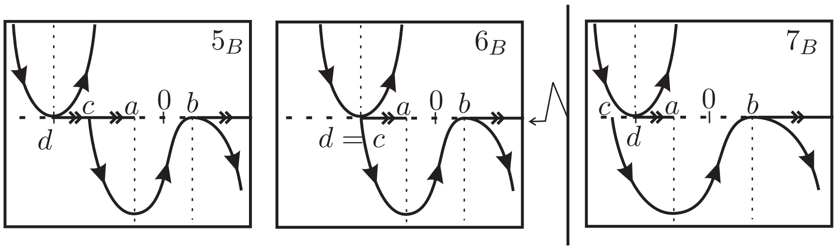

Figure 30. *Cases* 5_B*–*7_B*.*

$\diamond$ *Case* 8_B: $\lambda = -\sqrt{\beta}$. In this case $a = d$, and the configuration of the connected components of Σ is illustrated in Figure 31.

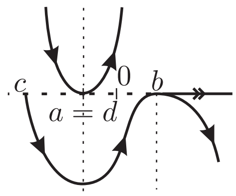

Figure 31. *Case* 8_B*.*

$\diamond$ *Case* 9_B: $-\sqrt{\beta} < \lambda < \sqrt{\beta}$. The points of Σ on the right side of b belong to Σ^e, and the points inside the interval (a, d) belong to Σ^s. The points on (d, b) and on the left of a belong to Σ^c. See Figure 32.

$\diamond$ *Case* 10_B: $\lambda = \sqrt{\beta}$. In this case $d = b$, and the configuration of the connected components of Σ is illustrated in Figure 32.

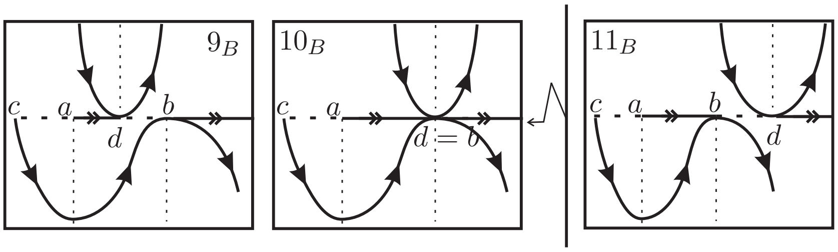

Figure 32. *Cases* 9_B–11_B.

⋄ *Case* 11_B: $\lambda > \sqrt{\beta}$. The points of Σ on the right of d belong to Σ^e, and the points inside the interval (a,b) belong to Σ^s. The points on (b,d) and on the left of a belong to Σ^c. See Figure 32.

The bifurcation diagram is illustrated in Figure 33. ■

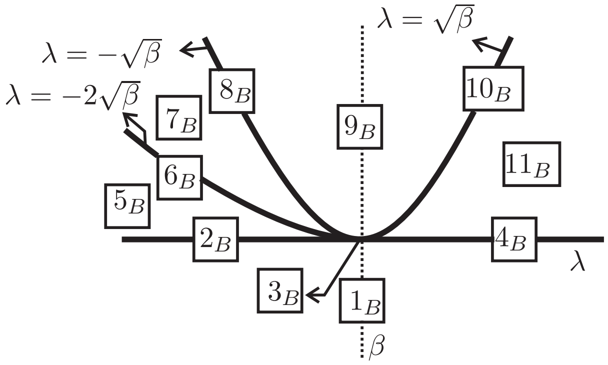

Figure 33. *Bifurcation diagram of Theorem* B.

8. Concluding remarks.

The results in section 12 of [9] were revisited and extended in this paper. The bifurcation diagram of a 3-parameter family of NSDSs presenting a fold-cusp singularity was exhibited. In particular, the existence of some new interesting global bifurcations around the standard fold-cusp singularity expressed by (2.1) was shown. Moreover, the simultaneous occurrence of such local and global bifurcations indicates how complex the behavior of this singularity is.

Acknowledgment. We would like to thank the referee for helpful comments and suggestions.

REFERENCES

[1] M. di Bernardo, C. J. Budd, A. R. Champneys, P. Kowalczyk, A. B. Nordmark, G. O. Tost, and P. T. Piiroinen, *Bifurcations in nonsmooth dynamical systems*, SIAM Rev., 50 (2008), pp. 629–701.

[2] M. di Bernardo, A. R. Champneys, S. J. Hogan, M. Homer, P. Kowalczyk, Yu. A. Kuznetsov, A. B. Nordmark, and P. T. Piiroinen, *Two-parameter discontinuity-induced bifurcations of limit cycles: Classification and open problems*, Internat. J. Bifur. Chaos Appl. Sci. Engrg., 16 (2006), pp. 601–629.

[3] M. di Bernardo, C. J. Budd, A. R. Champneys, and P. Kowalczyk, *Piecewise-Smooth Dynamical Systems—Theory and Applications*, Springer-Verlag, Berlin, 2008.

[4] C. A. Buzzi, T. de Carvalho, and P. R. da Silva, *Closed Poli-trajectories and Poincaré index of non-smooth vector fields on the plane*, J. Dynam. Control Systems, (2013), to appear.

[5] C. A. Buzzi, T. de Carvalho, and M. A. Teixeira, *On three-parameter families of Filippov systems—The fold-saddle singularity*, Internat. J. Bifur. Chaos Appl. Sci. Engrg., to appear.

[6] B. Coll, A. Gasull, and R. Prohens, *Center-focus and isochronous center problems for discontinuous differential equations*, Discrete Contin. Dynam. Systems, 6 (2000), pp. 609–624.

[7] A. F. Filippov, *Differential Equations with Discontinuous Righthand Sides*, Math. Appl., Kluwer Academic Publishers, Dordrecht, The Netherlands, 1988.

[8] P. Glendinning, *Non-smooth pitchfork bifurcations*, Discrete Contin. Dyn. Syst. Ser. B, 4 (2004), pp. 457–464.

[9] M. Guardia, T. M. Seara, and M. A. Teixeira, *Generic bifurcations of low codimension of planar Filippov systems*, J. Differential Equations, 250 (2011), pp. 1967–2023.

[10] V. S. Kozlova, *Roughness of a discontinuous system*, Vest. Moskov. Univ. Mat., 5 (1984), pp. 16–20.

[11] Yu. A. Kuznetsov, S. Rinaldi, and A. Gragnani, *One-parameter bifurcations in planar Filippov systems*, Internat. J. Bifur. Chaos Appl. Sci. Engrg., 13 (2003), pp. 2157–2188.

[12] M. A. Teixeira, *Generic bifurcation in manifolds with boundary*, J. Differential Equations, 25 (1977), pp. 65–88.

[13] M. A. Teixeira, *Generic singularities of discontinuous vector fields*, An. Acad. Brasil. Ciênc., 53 (1991), pp. 257–260.

[14] M. A. Teixeira, *Perturbation theory for non-smooth systems*, in Encyclopedia of Complexity and Systems Science 152, R. A. Meyers, ed., Springer, New York, 2009, pp. 6697–6719.

[15] S. M. Vishik, *Vector fields near the boundary of a manifold*, Vestn. Moskov. Univ. Mat., 27 (1972), pp. 21–28.